# TENSILE DEFORMATION AND FRACTURE BEHAVIOR OF $Ti_3Al$-Nb ALLOY AT HIGH TEMPERATURE①

Wu Ying, Zhen Liang, Yang Dezhuang
*School of Materials Science and Engineering, Harbin Institute of Technology, Harbin 150001*

**ABSTRACT** As $Ti_3Al$-base alloys have potentials used as high temperature structural material, the tensile deformation and fracture mechanism of Ti-24Al-14Nb-3V-0.5Mo(mole percent) alloy at high temperature was studied. The results indicate that there are considerable subgrain boundaries in the $\alpha_2$ and $B_2$-phases, which make the grain finer; the $\alpha_2/\alpha_2$ and $\alpha_2/B_2$ boundaries are vague and there are high density of dislocation tangles in the $B_2$-phase; the slip of $\boldsymbol{a}$-type dislocations on basal planes {0001} and prismatic planes $\{10\bar{1}0\}$ is the main deformation mode in the $\alpha_2$-phase apart from a few of $\boldsymbol{c}+\boldsymbol{a}/2$-type dislocations on pyramidal planes $\{0\bar{2}21\}$. The fracture of samples tensioned at 700 ℃ is of dimple type, and $\sigma_b$, $\sigma_{0.2}$, $\delta$ are 685 MPa, 580 MPa, 12.5% respectively.

**Key words** $Ti_3Al$-Nb alloy tensile deformation fracture

## 1 INTRODUCTION

$Ti_3Al$-base alloys have excellent potential as advanced high temperature structural materials for their high elevated temperature strength, good stiffness and high elastic modulus because of their low density and the long-range ordered arrangement of the constituent atoms in the crystal structure[1]. However, the lack of adequate independent slip systems and the low mobility of superlattice dislocations in the long-range ordered $DO_{19}$ crystal structure lead to the poor ductility of $Ti_3Al$ alloys at room temperature[2]. This limits their development and application in the field of aviation and aerospace. It has recently been shown that the addition of β-stabilizing elements such as Nb, Mo and V results in not only the retaining of the β-phase to room temperature, but also the slip of $\boldsymbol{c}+\boldsymbol{a}/2$-type dislocations on non-basal planes of the $\alpha_2$-phase, which ameliorates the ductility of $Ti_3Al$-base alloys[3]. The deformation and fracture mechanism of the $Ti_3Al$-Nb alloy being not understood, much work on tensile deformation, fatigue and fracture toughness behavior of the alloys at room temperature has been carried out[4-6]. While studies of high temperature deformation and fracture behavior of these alloys are seldom done. The microstructure features at high temperature and effect of test temperature on the deformation and fracture behavior of the alloy, and the fracture and dislocation configurations were investigated further in this paper.

## 2 EXPERIMENTAL

The nominal composition of the $Ti_3Al$-Nb alloy in this investigation is Ti-24Al-14Nb-3V-0.5Mo(mole percent). An ingot of the alloy was first melted by vacuum consumable electrode arc melting, and then forged in the β region. Finally, the $Ti_3Al$-Nb plates were cold-rolled to 1.7 mm in thickness and solution treated in the $\alpha_2$+β region at 1 000 ℃ for 1 h followed by water quenching (WQ) so as to attain the primary equiaxed $\alpha_2$-phase with a suitable volume fraction. High temperature tensile tests were carried out in an Instron testing machine at a tensile rate of 0.5 mm/min. The TEM foils were electropol-

① Received Apr. 9, 1996; accepted Sep. 26, 1996

ished to electron transparency in a twin jet electropolisher at - 20~ - 30 ℃ and a potential of 25~ 30 V in a solution of 15% ethanol, 70% butanol, 5% perchloric acid, 10% $H_2O$. The microstructure was examined with an optical microscope and a CM12 transmission electron microscope (TEM). The volume fraction of the primary $\alpha_2$-phase was measured with an autographical-analyser. The fractography was observed in a S-570 scanning electron microscope (SEM) and the dislocation structures were analysed by an H-800 TEM at a voltage of 200 kV.

## 3 RESULTS AND DISCUSSION

### 3.1 Microstructures before tensile deformation and mechanical properties of alloys

Fig. 1 shows microstructures of the specimen solution treated at 1 000 ℃ for 1 h followed by WQ before tensile deformation. It can be seen from Fig. 1(a) that the $\alpha_2$-phase shows equiaxed shape and distributes evenly in the $B_2$-phase matrix. The volume fraction of the primary $\alpha_2$-phase were measured to be about 30% with an auto- graphical-analyser. A typical TEM micrograph, which consists of the primary equiaxed $\alpha_2$-phase, $B_2$-phase and $O$-phase, is shown in Fig. 1(b). The formation of the $O$-phase in the alloy is due to the high Nb (14%) content, which makes Nb supersaturation in the primary $\alpha_2$-phase to form the $O$-phase. Selected area diffraction patterns (SADPS) of the $\alpha_2$-phase in [0001], the $B_2$-phase in [111] and the $O$-phase in [001] zone axis are also shown in Fig. 1(b) correspondingly. It is observed from the undeformed samples that there is almost no dislocation in the majority of primary $\alpha_2$ grains except for a few of dislocations on the $\alpha_2/B_2$ boundaries.

In addition, the results of room temperature tensile tests for samples solution treated at different temperatures indicate that the solution temperature controls the volume fractions of the primary $\alpha_2$-phase and thus effects the mechanical properties of the alloy. In short, it can be concluded that the mechanical properties at room temperature are in the best combinnation when the alloy is solution treated at 1 000 ℃, 1 h/WQ: $\sigma_b$= 984.5 MPa, $\sigma_{0.2}$= 785.5 MPa and $\delta$ = 5.9%.

### 3.2 Microstructures and mechanical properties in samples tensile deformed at high temperatures

Fig. 2 shows TEM micrographs of the alloy samples tensile deformed at 700 ℃ after solution


**Fig. 1 Micrographs showing microstructures of Ti-24Al-14Nb-3V-0.5Mo alloy solution treated at 1 000 ℃ for 1 h followed by WQ before tensile deformation**

(a) —optical microstructure; (b) —TEM microstructure

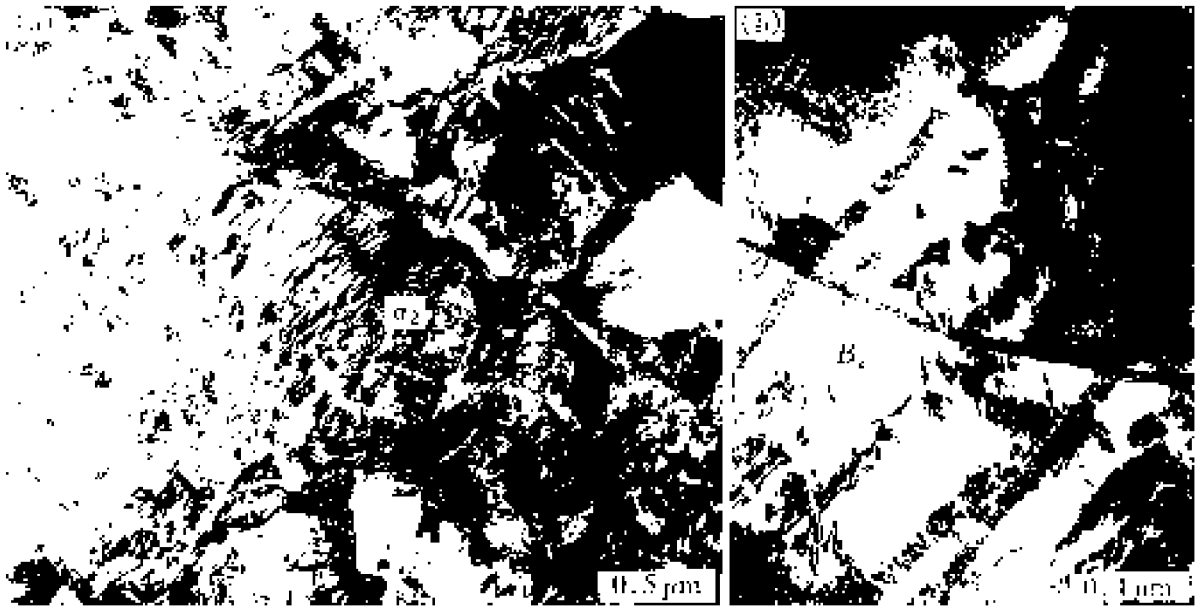

**Fig. 2 TEM micrographs showing microstructures of Ti-24Al-14Nb-3V-0.5Mo alloy after tensile deformation at 700 ℃**

(a) —TEM microstructure; (b) —high density dislocation tangles in $B_2$-phase

treated at 1000 ℃ for 1 h followed by WQ(1000 ℃, 1 h/WQ). It is obvious that the microstructures alter greatly(Fig. 2(a)). On one hand, the deformation is concentrated on the $B_2$-phase because the volume fraction of the primary $\alpha_2$-phase is lower, and there are high density of dislocation tangles in the $B_2$-phase (Fig. 2(b)) except for considerable subgrain boundaries in the $\alpha_2$ and $B_2$-phases; on the other hand, a few of secondary acicular $\alpha_2$-phases and a large number of $O$-phases are precipitated when the samples are heated and tensioned at 700 ℃, which produces short-time aging effect. Having been deformed greatly, the $\alpha_2/\alpha_2$ and $\alpha_2/B_2$ boundaries are vague and make the microstructures finer. During the deformation of grains and grain boundaries, a lot of interfacial dislocations are emitted from the $\alpha_2/B_2$ boundaries in order to coordinate the deformation of all grains.

In order to investigate the deformation mechanism of the primary $\alpha_2$-phase in samples tensile deformed at 700 ℃, slices were cut perpendicularly to the tensile axis from the gage length part of tensile specimens and polished to TEM foils. Dislocation structures and slip systems were analyzed in accordance with the $\boldsymbol{g}\cdot\boldsymbol{b}=0$ invisibility criterion in an H-800 TEM equipped with a side entry gonimeter stage capable of ±45° tilting on the X or Y axis, and several bright and dark field micrographs with different operating reflections $\boldsymbol{g}$ were chosen. Fig. 3 shows a series of diffraction contrast micrographs in the same $\alpha_2$ grain, it is obvious that there are hexagonal dislocation networks in the primary $\alpha_2$ grain. A series of two-beam micrographs were obtained with operating reflections of $\boldsymbol{g}=0\bar{1}10$, $\bar{2}202$, $\bar{1}011$ in $[\bar{2}113]$; $\boldsymbol{g}=\bar{1}010$, $\bar{1}100$ in $[0001]$ and $\boldsymbol{g}=0\bar{1}11$ in $[\bar{1}123]$ zone axis so as to determine the $\boldsymbol{b}$ of hexagonal dislocation networks. Because $A$ group dislocations are invisible with $\boldsymbol{g}=0\bar{1}10$ (Fig. 3(a)) and $\boldsymbol{g}=0\bar{1}11$ (Fig. 3(f)), therefore, it is determined that $A$ group dislocations are $\boldsymbol{a}$-type ones with $\boldsymbol{b}=1/6[\bar{2}110]$; $B$ group dislocations are invisible with $\boldsymbol{g}=\bar{1}011$ (Fig. 3(c)) and $\boldsymbol{g}=\bar{1}010$ (Fig. 3(d)), showing the $\boldsymbol{b}$ of $B$ group dislocations is $1/6[\bar{1}2\bar{1}0]$. $A$ and $B$ group dislocations react with each other to form $C$ group dislocations with a $\boldsymbol{b}=1/6[\bar{1}\bar{1}20]$. The formation of hexagonal dislocation networks is due to the result of dislocation reactions. During the deformation process, there is stress concentration at grain boundaries, which leads to the emition of dislo-

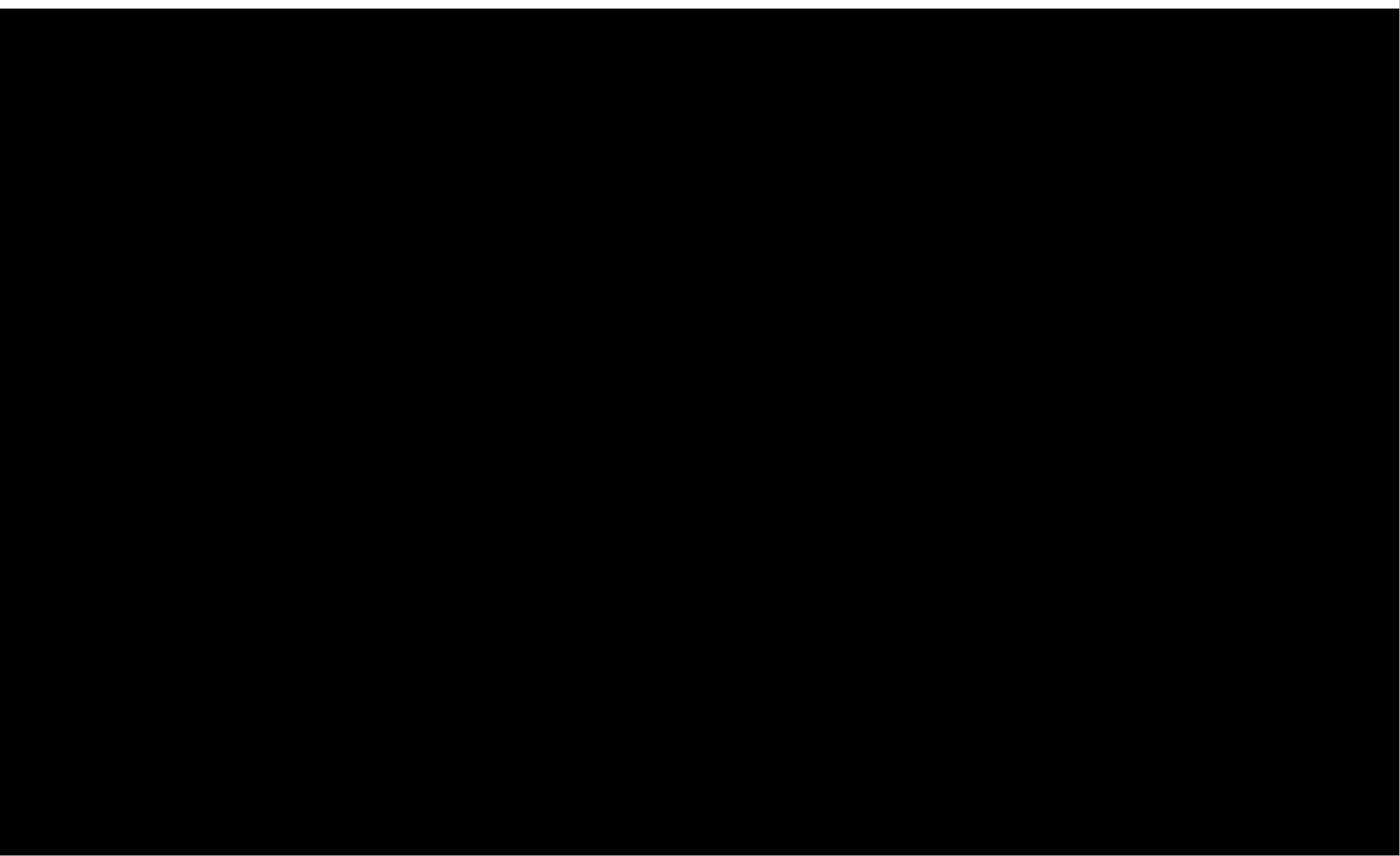

**Fig. 3 TEM micrographs showing hexagonal dislocation networks formed by *a*-type dislocations in primary $\alpha_2$ grain after tensile deformation at 700 ℃**

(a) $-\boldsymbol{g}=0\bar{1}10$; (b) $-\boldsymbol{g}=\bar{2}202$; (c) $-\boldsymbol{g}=\bar{1}011$; (d) $-\boldsymbol{g}=10\bar{1}0$; (e) $-\boldsymbol{g}=\bar{1}100$; (f) $-\boldsymbol{g}=0\bar{1}11$

cations to relax the stress and coordinate peripheral strain. When two rows of dislocations with an angle of 120° (marked as *P* in Fig. 3(b)) meet together, these dislocations can react to form hexagonal dislocation networks, which can be expressed as $1/6[\bar{2}110] + 1/6[\bar{1}2\bar{1}0] = 1/6[\bar{1}\bar{1}20]$. The analysis of the trace shows that the distance between *A* and *A* group dislocations (or between *B* and *B* group dislocations) is the largest (Fig. 3(d), 3(e)) when the foil orientation is close to the [0001] zone axis. Therefore, the slip planes of ***a***-type dislocations are basal planes {0001}.

Fig. 4 shows another dislocation diffraction

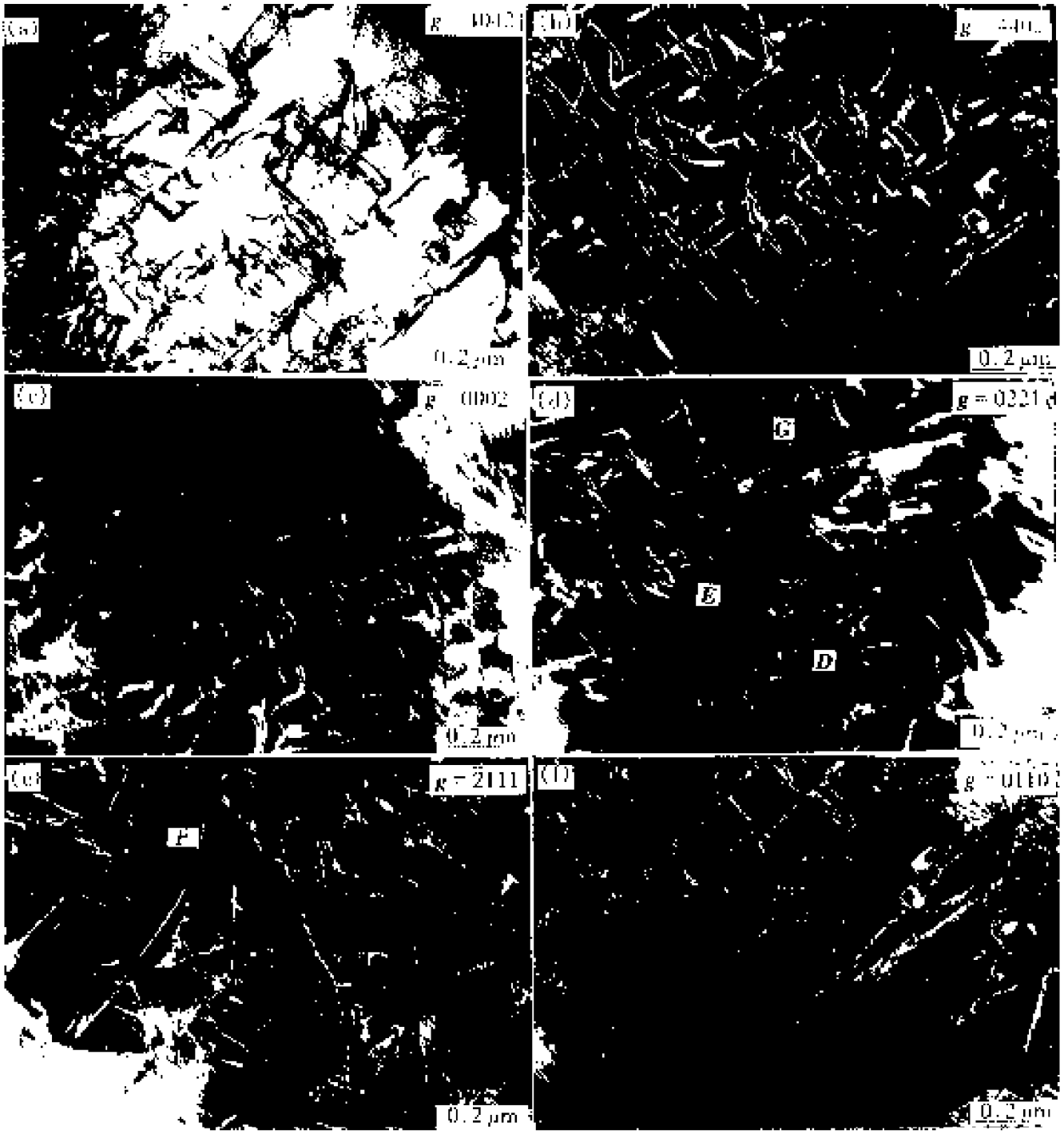


**Fig. 4 TEM micrographs showing dislocation structures in the primary $\alpha_2$ grains after tensile deformation at 700 ℃**

(a) $-\boldsymbol{g} = 40\bar{4}2$; (b) $-\boldsymbol{g} = 4\bar{4}02$, dark field image of $\boldsymbol{c}+\boldsymbol{a}/2$-type dislocation pairs; (c) $-\boldsymbol{g} = 0002$; (d) $-\boldsymbol{g} = 0\bar{2}21$; (e) $-\boldsymbol{g} = \bar{2}111$; (f) $-\boldsymbol{g} = 01\bar{1}0$

contrast micrographs in the primary grains, with operating reflections of $\boldsymbol{g}$= 0002, 01$\bar{1}$1, 44$\bar{0}$4, 01$\bar{1}$0, $\bar{1}$011, $\bar{2}$111, 44$\bar{0}$2, 02$\bar{2}$1, $\bar{1}$010, 40$\bar{4}$2. Because the lattice parameters of the $\alpha_2$-phase are very large ($a$= 0.577 nm, $c$= 0.462 nm), it is difficult to obtain an ideal two-beam condition. Sometimes higher index spots or weak-beam conditions were used. In general, $\boldsymbol{a}$-type dislocations with $\boldsymbol{b}$= 1/6[$\bar{1}$120], and $\boldsymbol{c}$+ $\boldsymbol{a}$/2-type dislocations with $\boldsymbol{b}$= 1/6[$\bar{1}$126] are superdislocations, but $\boldsymbol{c}$-type dislocations with $\boldsymbol{b}$= 1/3[0003] are not. $\boldsymbol{c}$+ $\boldsymbol{a}$/2-type dislocations usually exist in the form of dislocation pairs. It has been found that there are $\boldsymbol{c}$+ $\boldsymbol{a}$/2-type or $\boldsymbol{c}$-type dislocations in the form of kinks in Fig. 4 (a). When $\boldsymbol{g}$= 40$\bar{4}$2 (Fig. 4(a)) and $\boldsymbol{g}$= 44$\bar{0}$2 (Fig. 4(b)), $D$ and $E$ dislocation pairs are both invisible, while other diffraction micrographs are still visible, therefore, it is determined that the $\boldsymbol{b}$ of $D$ and $E$ dislocation pairs is parallel to [$\bar{1}$126]. According to the lowest energy principle, $D$ and $E$ dislocation pairs belong to superpartial dislocation pairs with $\boldsymbol{b}$= 1/6[$\bar{1}$126]. Fig. 4(c) shows a dark field image with $\boldsymbol{g}$= 0002, in which most dislocations are invisible (such as $F$ and $G$). It is observed that $\boldsymbol{a}$-type dislocations are the majority and $\boldsymbol{c}$+ $\boldsymbol{a}$/2-type dislocations are the minority and no $\boldsymbol{c}$-type dislocations are found (Fig. 4(a) ~ 4(f)). Because the slip planes of the $\boldsymbol{a}$-type dislocations are usually the prismatic and basal planes and those of the $\boldsymbol{c}$ + $\boldsymbol{a}$/2-type dislocations are pyramidal ones. The result of analysis shows that $F$ dislocations slip on the ($\bar{0}$110). When the electron beam close to the [02$\bar{2}$1] zone axis, the spacing distances of $D$ and $E$ dislocation pairs are the largest (Fig. 4(d)), that is to say, the slip planes of $D$ and $E$ dislocation pairs are (02$\bar{2}$1).

Fig. 5 shows the tensile properties as a function of the deformation temperature. Obviously, with the deformation temperature increasing, the strengths decrease, but the elongation increases gradually and the strengths decrease and the elongation increases greatly between 300 and 500 ℃, which indicates that hardening rate between 500 and 700 ℃ is larger. Although the strengths at 700 ℃ decrease by 200 MPa than those at room temperature, $\sigma_b$= 685 MPa, $\sigma_{0.2}$ = 580 MPa, the strengths at 700 ℃ still maintain higher level, the elongation nearly doubles, $\delta$= 12.5%.

### 3.3 Tensile fractography

Fig. 6 shows the room temperature (Fig. 6

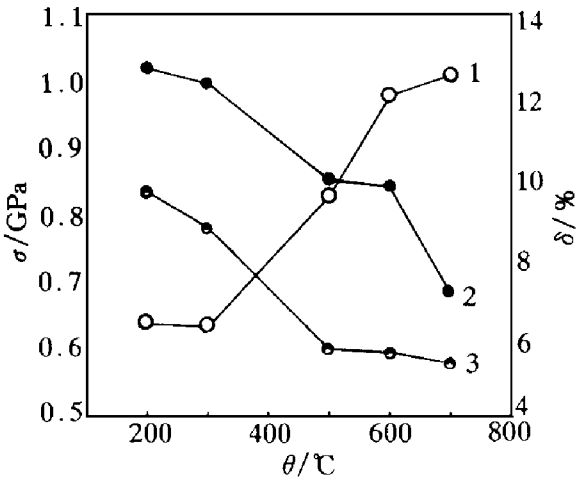


**Fig. 5 Change of tensile properties of Ti-24Al-14Nb-3V-0.5Mo alloy with test temperatures**

1—$\delta$; 2—$\sigma_b$; 3—$\sigma_{0.2}$

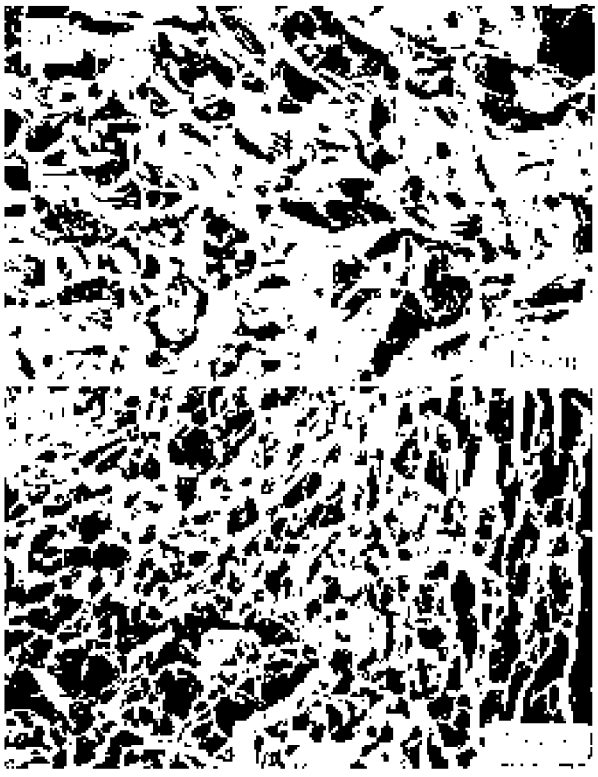

**Fig. 6 SEM fractography of Ti-24Al-14Nb-3V-0.5Mo alloy**

(a) —room temperature; (b) —700 ℃

(a)) and 700 ℃ (Fig. 6(b)) tensile fractography of the $Ti_3Al$-Nb alloy after solution treated at 1 000 ℃ for 1 h followed by WQ. Fig. 6(a) shows that the fracture of specimens tensioned at room temperature is a mixed one, which consists of both the brittle cleavage fracture characterized by cleavage facets and river markings, and the ductile one characterized by dimples and tear ridges. While, the specimen tensioned at 700 ℃ shows only dimple-type failure (Fig. 6(b)), infering that the elongation of the specimen increases.

## 4 CONCLUSIONS

(1) After tensile deformation at 700 ℃, considerable subgrain boundaries are formed, which makes grains finer; the $\alpha_2/\alpha_2$ and $\alpha_2/B_2$ boundaries are vague and there are high density of dislocation tangles in the $B_2$-phase; the slip of ***a***-type dislocations on basal planes {0001} and prismatic planes $\{10\bar{1}0\}$ is the main deformation mode in the $\alpha_2$-phase, while a few ***c*** + ***a***/2-type dislocations can also be observed on pyramidal planes $\{0\bar{2}21\}$.

(2) The strength decreases and the elongation increases with the tensile test temperature increasing; the fracture of specimens tensioned at room temperature consists of cleavage patterns, dimples and tear ridges, while the fracture of specimen tensioned at 700 ℃ shows only dimple feature.

## REFERENCES

1 Lipsitt H A. In: Koch CC, Liu C T and Stoloff N S, ed. High-Temperature Ordered Intermetallic Alloys. Pittsburgh: Materials Research Society, 1985, Vol. 39, 351- 364.
2 Lipsitt H A, Schechtman D, Schafrik. Metall Trans A, 1980: 1369- 1375.
3 Gogia A K, Banerjee D, Nandy T K. Metall Trans A, 1990, (21A): 609- 625.
4 Sun F S, Gao W, Cao C X. Journal of Aeronautical Materials, (in Chinese), 1995, 6(2): 14- 20.
5 Lin T H, Chen T H. Mater Sci Eng A, 1993: 103- 110.
6 Chen K S. Metall Trans A, 1993, (24A): 569- 583.

**(Edited by Huang Jinsong)**